Bulletin of the Seismological Society of America, 91, 4, pp. 781–791, August 2001

Source Characteristics of a 5.5 Magnitude Earthquake that Occurred in the Transform Fault System of the Delfin Basin in the Gulf of California

by Cecilio J. Rebollar, Luis Quintanar, Raul R. Castro, Steven M. Day, Juan Madrid, James N. Brune, Luciana Astiz, and Frank Vernon

Abstract Portable and permanent broadband seismic stations in the neighborhood of the Gulf of California recorded a moment magnitude M_w 5.5 event on 26 November 1997. This is the first time that a moderate event located in the Gulf of California extensional province was well recorded by local broadband seismic stations. The event was located at 29.754° N and 113.708° W and at a focal depth of 5.0 km in the southeastern end of the transform fault that connects the lower and upper Delfin basins. The hypocentral location and the results of the wave modeling indicate that this is a complex event that originated in the pull-apart Delfin basin. The focal mechanism estimated from first motions ($\phi = 310°$, $\delta = 83°$, $\lambda = 97°$) and body-wave modeling of *P* waves in the frequency band 0.05–0.5 Hz suggests that the rupture started with dip-slip (reverse faulting) motion and ended releasing the bulk of energy through strike-slip motion. Synthetics of surface waves in the frequency band 0.05–0.1 Hz were also calculated using a triangular source–time function of 3 sec. The best match between the synthetics and observed surface waves recorded at 90 km from the epicenter was obtained using a fault geometry defined by a strike of 330° ± 15, dip 85° ± 5, and slip of 165° ± 15.

The spectral analysis of the *Lg* phase recorded at stations in the Peninsular Ranges gives a seismic moment of 1.28×10^{17} N m (1.28×10^{24} dyne cm), a source radius of 6.3 km and a stress drop of 0.22 MPa (2.2 bar). The source parameters inferred with *S*-wave spectra and the same model (Brune, 1970) give similar values.

Introduction

In October 1997, we deployed 11 broadband seismic stations in Northern Baja California across an E–W line at about 31° N, in a joint study between North American and Mexican scientists to study crustal thickness in Northern Baja California (Fig. 1). The North Baja Transect (NBT) stations consisted of Guralp broadband seismometers (CMG-40T and CMG-3ESP) connected to REFTEK high-resolution digitizers and peripherals from the following institutions: Centro de Investigación Cientifica y de Educación Superior de Ensenada (CICESE), PASSCAL, Southern California Earthquake Center (SCEC), University of Nevada at Reno (UNR), University of California, San Diego (UCSD), and San Diego State University (SDSU). The NBT stations recorded continuously from October 1997 to July 1998. On 26 November 1997, a M_w 5.5 earthquake occurred in the extensional province of the Gulf of California. This earthquake was located northwest of Angel de la Guarda Island, along the transform fault that connects the lower Delfin basin with the upper Delfin basin (Fig. 1). These basins were previously defined by Lommnitz *et al.* (1970) using bathymetry contours of the Gulf of California. The NBT seismic stations as well as the permanent short period stations of Red Sísmica del Noroeste de México (RESNOM) and STS-2 broadband seismic stations at Bahia de Los Angeles (BAHI), Guaymas (GUAY), and Tucson (TUC) recorded the Delfin earthquake.

Because of the lack of local and regional stations, earthquakes reported by ISC and NEIC with magnitudes less than 5.0 do not show a defined pattern in the upper region of the Gulf of California. This is the first time that a moderate event in the Gulf of California was recorded by nearby modern broadband digital seismic stations. In this study we report the location, fault geometry, and source parameters of this event.

Tectonic Setting

The Gulf of California is part of the boundary between the North American and Pacific plates. Lomnitz *et al.* (1970) proposed a simple idealized tectonic framework of northwest–southeast strike-slip faults separated by northeast–southwest spreading centers. More recently, Tajima and Tralli (1992) describe a north–south gradation in the tectonic

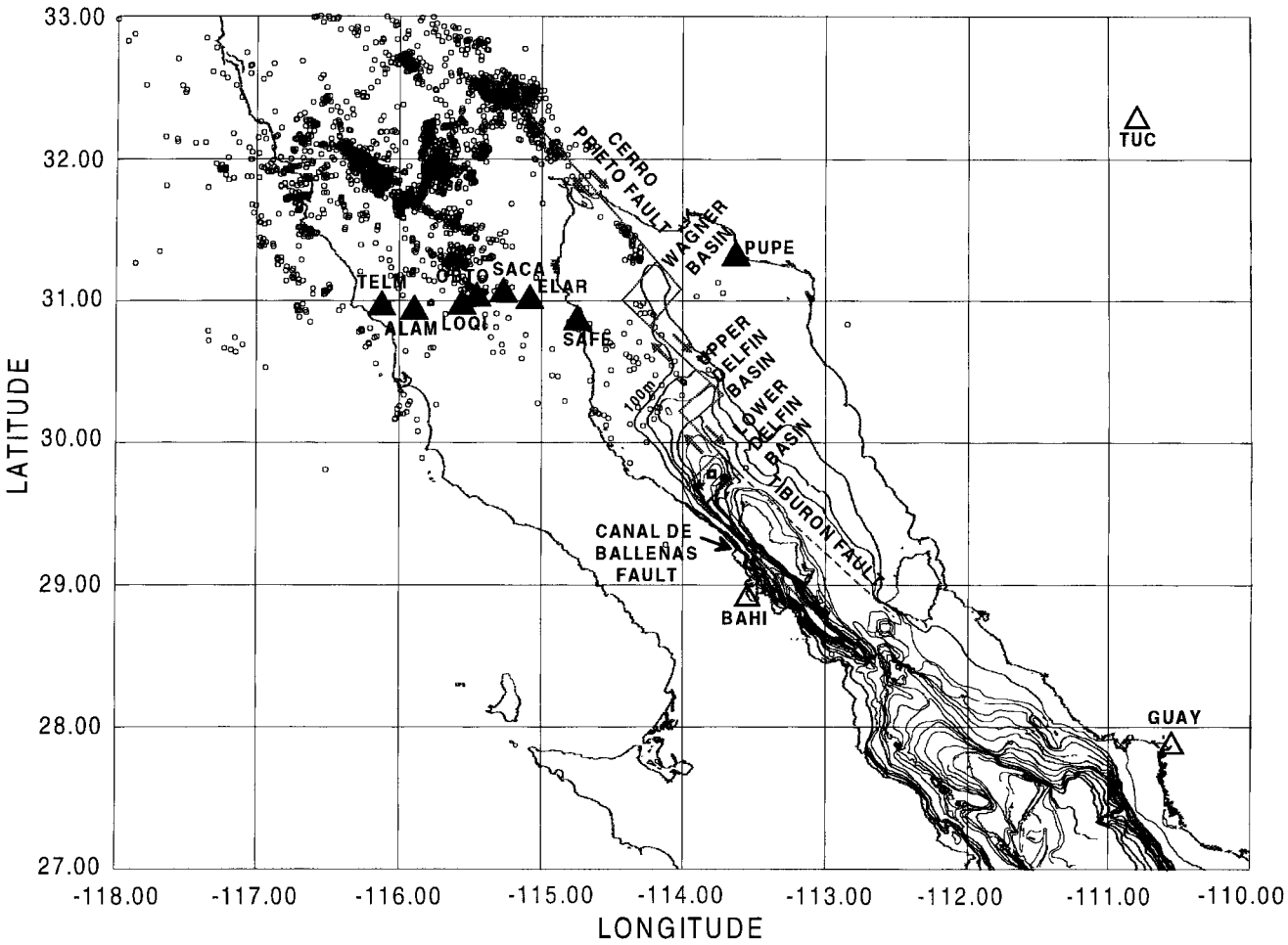

Figure 1. Map of Northern Baja California and the extensional province of the Gulf of California showing the bathymetry (depth contours every 100 m), the idealized tectonic framework of strike-slip and spreading centers from Lomnitz *et al.* (1970), and the locations of the seismic stations. Solid triangles are NBT stations and open triangles are the permanent broadband stations. Also shown is the Tucson station (TUC). Open circles are the epicenters from the RESNOM catalog. Solid circle shows our location of the Delfin earthquake, open square is the ISC location and solid star is the NEIC location.

character of the Gulf of California. They recognize the following tectonic elements: a ridge-transform fault system in oceanic crust in the southernmost portion of the Gulf; a transition zone between oceanic and continental crust in the southern and central Gulf; and a transitional extension–transform system in the northern Gulf, which becomes the San Andreas system in southern California. They also found that the seismic to tectonic slip ratios are low, increasing slightly from south to north. This observation contrasts with the relatively high rates of seismic activity in the south relative to the north of the Gulf of California.

The northern Gulf of California consists of the Wagner and Upper and Lower Delfin Basins, connected by inferred transform faults that have not been delineated by seismic activity. Angel de la Guarda Island, located to the southeast of the Lower Delfin Basin, is bounded by the Canal de Ballenas, a transform fault on the southwest and the abandoned Tiburon transform fault on the northeast (Lonsdale, 1989). This region lies within the Gulf of California extensional province (see Fig. 1).

Seismicity

The RESNOM network routinely locates background seismic events between 30° N and 32° N. Figure 1 shows events located by RESNOM. The International Seismological Center (ISC) and PDE earthquake locations in the Gulf of California are also scattered. Although the seismicity in the Cerro Prieto transform fault region is well located, less reliable locations are determined further south in the Gulf of California, specially south of the Wagner basin.

Previous studies of microearthquake activity in this region of the Gulf of California were done by Lomnitz *et al.* (1970), Thatcher and Brune (1971), and Reichle and Reid

(1977). Their results showed that the activity occurred mostly as earthquake swarms in the Wagner and Delfin basins; the depths of the events were not deeper than 7 km, and the focal mechanism of a 5.4 magnitude event located in the Wagner basin was consistent with normal faulting. Goff *et al.* (1987) determined source characteristics of events from the Gulf of California recorded at teleseismic distances. They found that events located in spreading centers showed normal faulting, and events located in transform faults were characterized by right-lateral strike-slip faulting.

Earthquake Location

We located the Delfin earthquake with the HYPOCENTER (Lienert *et al.,* 1988; Lienert and Havskov, 1995) as well as the HYPO71 (Lee and Lahr, 1972) programs using the one-dimensional crustal model obtained by Gonzalez *et al.* (1998). This crustal velocity model was calculated from a refraction study carried out from the Delfin basin to seismic station SAFE (see Fig. 1). The model has a thin continental crust with a Moho depth in the range from 20 to 24 km (see Table 1). Thatcher and Brune (1973) calculated an average crustal structure from surface waves traveling along the Baja California peninsula and through marine paths. The velocity model calculated with surface waves traveling along the Baja California peninsula has a crustal thickness of 25 km. On the other hand, the velocity model obtained from marine paths is 16 km thick and differs by 8 km from the velocity model reported by Gonzalez *et al.* (1998). More recently, Lewis *et al.* (2001) and Reyes *et al.* (2001) found that the Moho depth increases from 20 km near the Gulf of California to 44 km along the batholith of the Peninsular Ranges, then decreases again to 34 km toward the Pacific Ocean. In this article we located the Delfin event using *P*-wave arrivals of the NBT and RESNOM stations and *P*- and *S*-wave readings from BAHI, SAFE, and GUAY, the closest stations to the epicenter. We also used *P*-wave arrivals from the station Tucson (TUC). We fixed the focal depth at 10 km and found that HYPOCENTER and HYPO71 gave similar locations, although with large residuals. Residuals slightly decreased when the focal depth was located close to the surface. When we located the event with *P* and *S* waves of the stations BAHI, SAFE, ELAR, TUC, and GUAY, the epicentral location did not changed greatly; however, the residuals were minimum at a depth of 5 km. The event was located at 29.754° N and 113.708° W with a fixed focal depth of 5.0 km. The depth was also constrained using surface-wave modeling. Horizontal and vertical errors are of the order of ±5 km. NEIC located the event at 29.70° N and 113.88° W with a depth of 10 km (no errors reported) and ISC at 29.78° N and 113.80° W with horizontal errors of the order of ±6.0 km with a depth of 10 km. The maximum distance between our location and NEIC and ISC locations are 17.0 and 9.5 km, respectively. Figure 1 shows our location and the NEIC and ISC locations of the event.

Table 1
Velocity Model Used to Locate the Event and *Q* Model Used in the Body- and Surface-Wave Modeling

Layer Thickness (km)	*P*-Wave Velocity (km/sec)	*S*-Wave Velocity (km/sec)	Density (g/cm^3)	Q_α	Q_β
4.0	4.0	2.6	1.8	400	200
4.0	5.7	3.3	2.5	2000	2000
16.0	6.7	3.8	3.0	2000	2000
0	7.8	4.0	3.4	2000	2000

Focal Mechanism

The focal mechanism was calculated with *P*-wave first motions from NBT and the permanent stations of RESNOM. We also used *P*-wave first motions from TUC, as well as from Mazatlan (MAIG), La Paz (LPIG), and Zacatecas (ZAIG) broadband seismic stations of the Servicio Sismológico Nacional de México. The focal mechanism solution was calculated with the program FPFIT (Reasenberg and Oppenheimer, 1985). Figure 2a and b shows the output of FPFIT in lower-hemisphere equal-area projections. There are two possible fault-plane solutions, one is a dip-slip reverse faulting with a vertical plane striking northwest–southeast (Fig. 2a), and the second is a strike slip with almost a north–south plane dipping to the west (Fig. 2b). The dip-slip solution shows a reasonable fit, even though picks are close to the nodal planes. The uncertainties in *P* and *T* axes are because most of the seismic stations are close to nodal planes, and FPFIT assigns a low weight to polarities close to nodal planes in the inversion process. We prefer the fault-plane solution that gives a strike $\phi = 310°$, dip $\delta = 83°$, and slip $\lambda = 97°$ because those values of ϕ and δ constrain the fault well and are consistent with the change in polarity from dilatation at ELAR to compression at SACA (Fig. 3a). In addition, the direction of the strike agrees with the orientation of the transform fault that connects the lower and upper Delfin basins (Lomnitz *et al.* 1970; Lonsdale 1989; Stock and Hodges, 1989). Figure 3b shows arrival times and *P*-wave polarity picks at GUAY, MAIG, and ZAIG, broadband seismic stations to the southeast of the epicenter. Those polarity picks constrain again the same nodal plane in the southeast. Station GUAY is a nodal station where the first arrival could be either up or down. We choose up, but, in both cases the fault-plane solution is constrained. The distribution of *P*-wave polarities favors reverse faulting with small uncertainties. The second possible fault plane solution (Fig. 2b) is strike slip but with larger uncertainties. However, this solution makes more sense from the geological point of view. The dip-slip solution is rather surprising since most earthquakes reported in the region are generated by normal or strike-slip faulting (Goff *et al.* 1987). In order to analyze if the rupture initiated as dip slip or strike slip, we modeled *P* and surface waves with both fault mechanisms. Body-wave modeling showed that the initial rupture started as a dip slip (fault plane solution shown in Fig. 2a). This apparent discrepancy with the

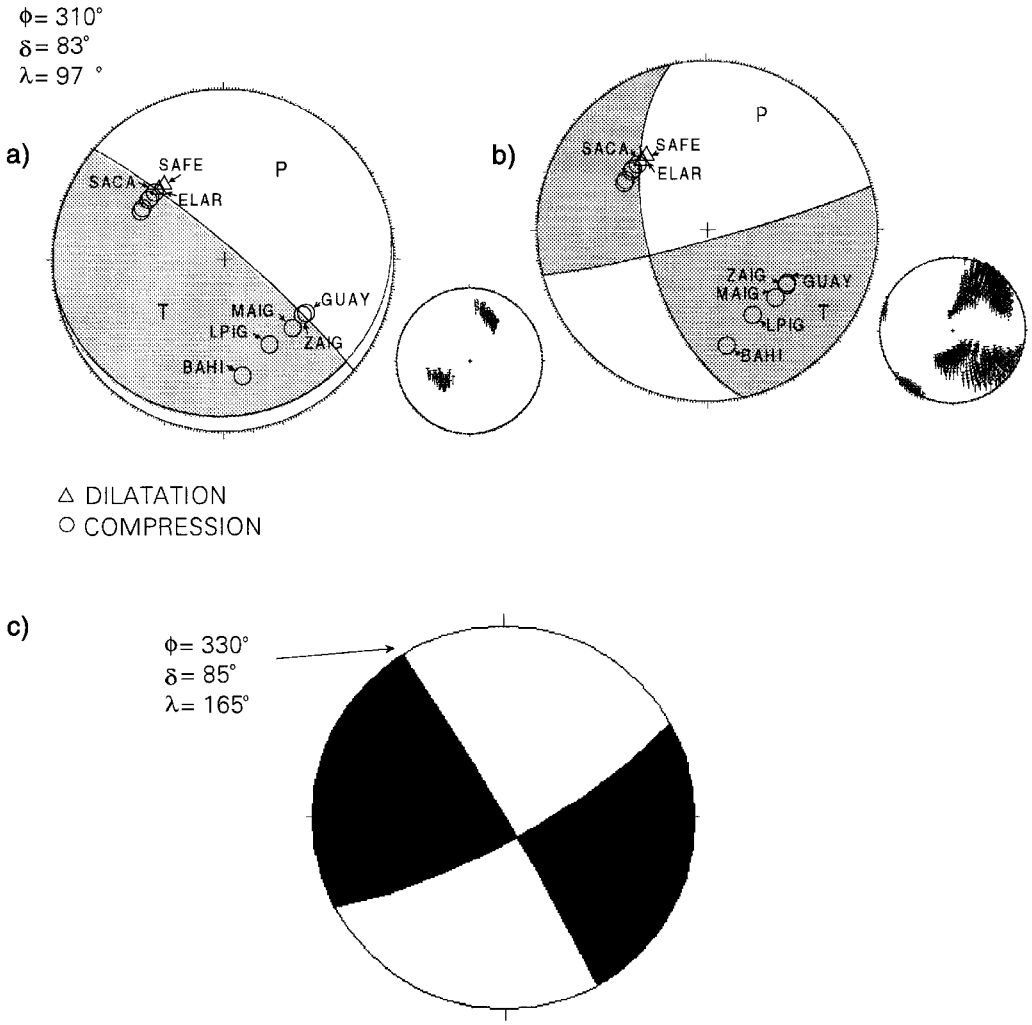

Figure 2. Focal mechanisms calculated with the FPFIT (Reasenberg and Oppenheimer, 1985) program and presented in a lower-hemisphere equal-area projection. The fault geometry is constrained with the change in polarity of stations ELAR and SACA in the northwest, and by stations GUAY and ZAIG (22.768°–102.567°) stations in the southeast. Circles not identified in the fault plane solution are OBTO, LOQI, ALAM, and TELM. There are two possible solutions: (a) dip-slip solution and (b) strike-slip solution. (c) Fault-plane solution obtained by waveform modeling of surface waves.

expected mechanism from the analysis of previous earthquakes in this zone may be explained by the complexity of this earthquake. It is possible that its initial rupture started as a dip slip. The later part of the rupture, as inferred from surface-wave modeling from the BAHI, SAFE, and GUAY stations and teleseismic Harvard CMT solutions (strike 329°, dip 86°, and slip 172°, Fig. 2c), ended as right-lateral strike-slip faulting.

Regional Modeling

P Waves

Regional *P*-wave displacement synthetics were computed using the discrete wavenumber representation of Green functions (Bouchon, 1981) with the velocity model obtained by González *et al.* (1998) and Lewis *et al.* (2001) for this region (see Table 1). Both synthetic and observed records were filtered with a causal bandpass butterworth filter between 0.05 and 0.5 Hz in order to include in the passband the corner frequency of the earthquake (0.2 Hz), obtained from *Lg* spectral analysis as discussed in a later section. Special attention was given to window selection in order to include only the *P*-wave arrival so that we could distinguish clearly the contributions from dip-slip and strike-slip faulting. We modeled the three components of the *P*-wave displacement records at three broadband regional stations (BAHI, SAFE, and GUAY) located around the epicenter (see Fig. 1). Epicentral distances range from 90 to 370 km. Since the main purpose is to identify the mechanism that best fits the beginning of the records, we calculated two sets

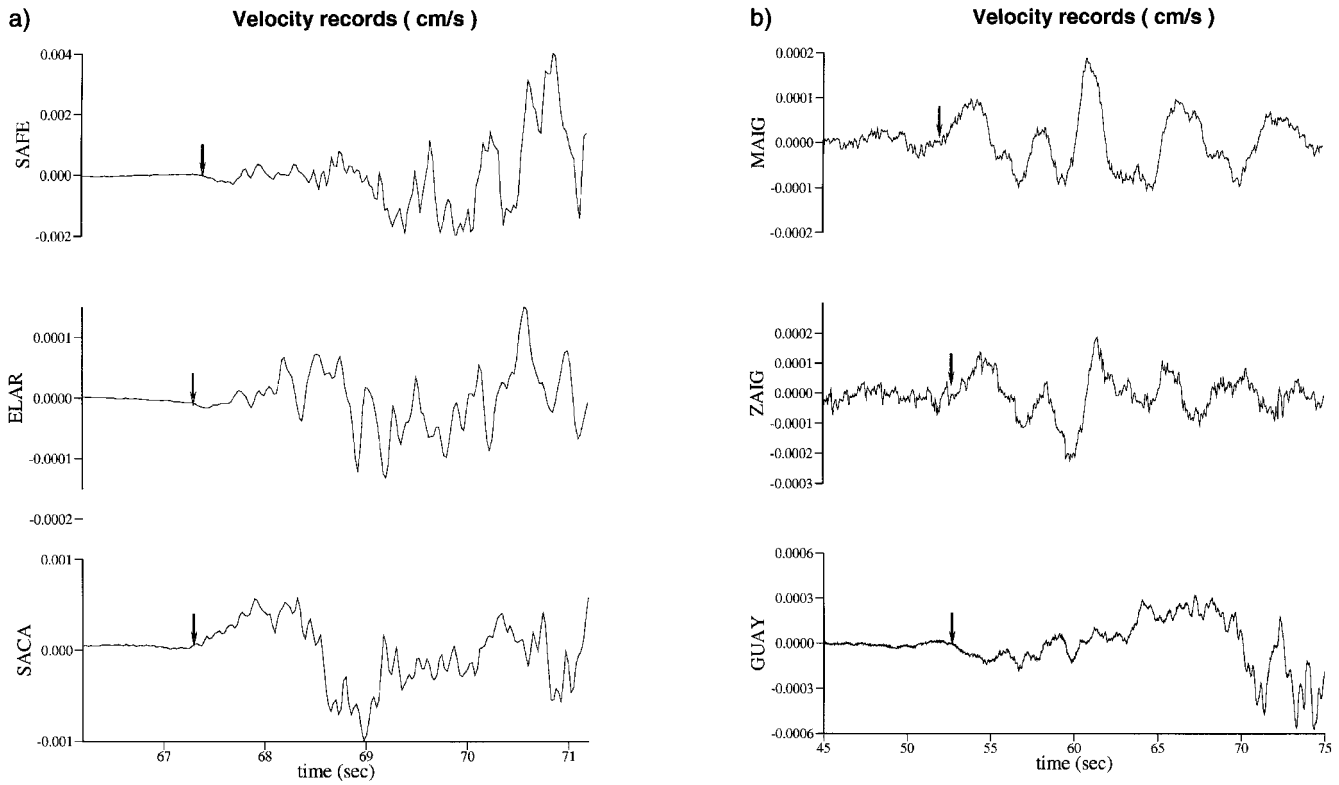

Figure 3. (a) Change in polarity at stations ELAR and SACA that constrain one fault plane in the focal mechanism. Arrows indicate the *P*-wave arrival and the polarities. (b) *P*-wave polarity at the broadband MAIG, ZAIG, and GUAY stations, located to the southeast of the epicenter.

of synthetics: one with the mechanism determined with the *P*-wave polarities ($\phi = 310°$, $\delta = 83°$, $\lambda = 97$), and the other with the mechanism from the Harvard group ($\phi = 329°$, $\delta = 86°$, $\lambda = 172°$). Integration of the BAHI seismograms gives a 3-sec triangular source–time function, similar to the source–time function duration of 2.4 sec reported by Harvard. Synthetics with both geometries, a 3-sec triangular source–time function, a seismic moment of 1.00×10^{17} N m, and variable depths were calculated.

Because of the epicentral distances to stations SAFE and GUAY (160 and 370 km respectively), the recorded wave motions are contaminated by the local structure. Therefore, it was necessary to apply a filter whose high-frequency cutoff value depends on the epicentral distance to the station in order to eliminate those undesirable contributions. Therefore, the data for the stations SAFE and GUAY were filtered at 0.1 and 0.5 Hz, respectively. On the other hand, we carefully included the corner frequency into the frequency band analyzed in the modeling process, because it is well known that the corner frequency of the source displacement spectrum is located at periods between the rise time and the rupture time. By doing this, we expect to retrieve the source information from the modeling process. Because BAHI is the nearest to the source (90 km), we did not apply any filter to the displacement record in our analysis. We were interested to determine whether the beginning of the rupture had a contribution of dip-slip faulting, and for this reason we modeled 5 sec of the signal at BAHI, SAFE, and GUAY stations. According to the corner frequency calculated from the spectral analysis, the rupture was completed within the first 5 sec at most. The vertical, radial, and tangential components of BAHI show a good agreement in the first 3 sec (see Fig. 4). The vertical component of GUAY (Fig. 5) and radial component of SAFE (Fig. 6) show a good agreement between synthetic and observed seismograms in the first 2 sec suggesting that the beginning of the rupture is well matched with a dip-slip faulting. The best fit was obtained with a source at a depth of 5 km. The result of this process is shown on Figures 4, 5, and 6, where it is also shown the synthetics with the Harvard solution, where we can see the mismatch with the strike-slip motion.

Surface Waves

We used the strike and dip of the fault-plane solution that agrees with the Delfin transform fault and searched for the slip through synthetic wave forward modeling. Synthetic seismograms were calculated with Herrmann's (1987) programs that use the theory presented by Wang and Herrmann (1980) and Herrmann and Wang (1987). The programs calculate 10 basic Green's functions, as a function of wavenumber and frequency, for a burled point source in a plane-

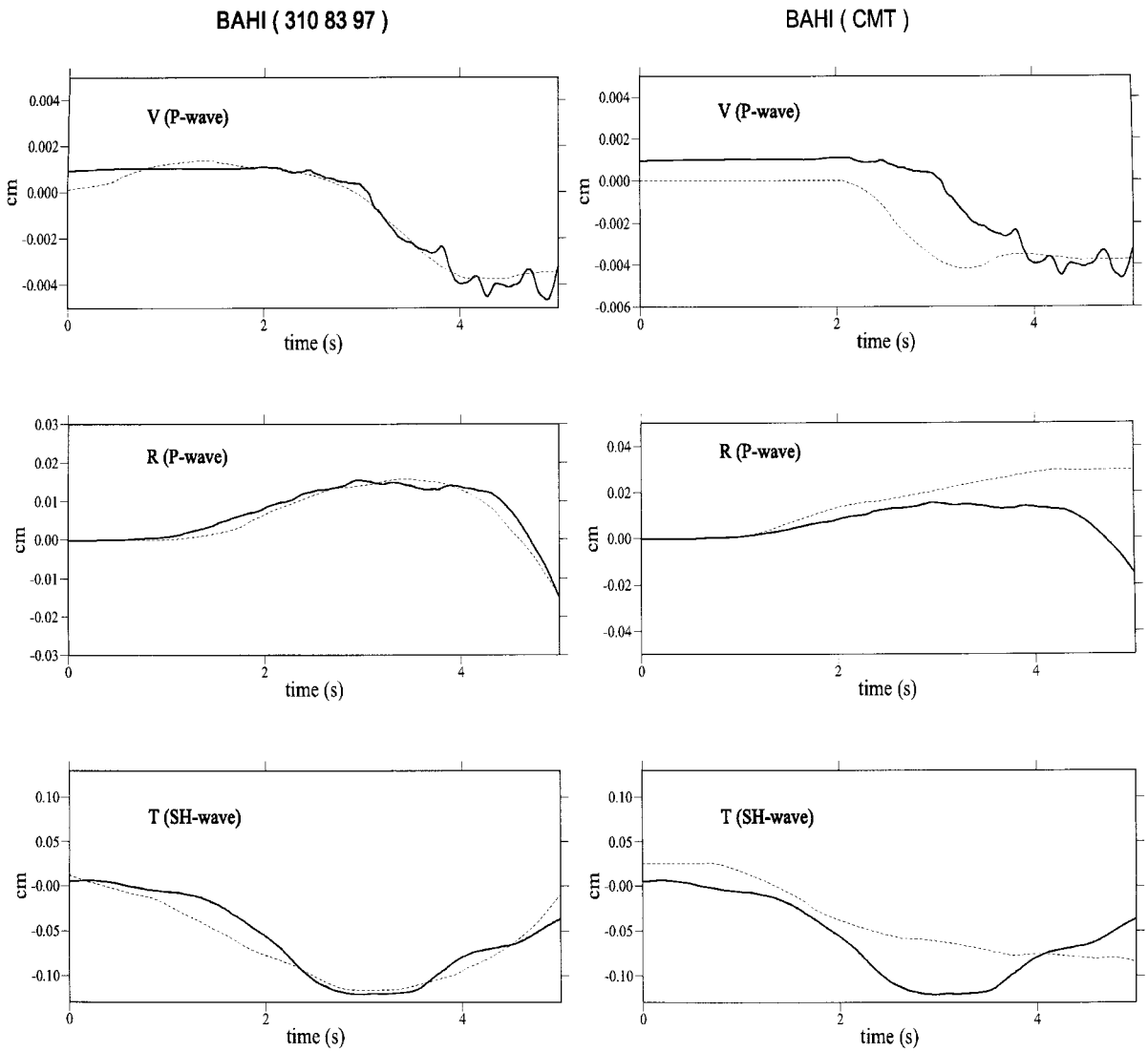

Figure 4. Comparison of observed and synthetics *P* waves calculated with the dip-slip geometry (left) and Harvard CMT (right) at BAHI station. The top of the figure indicates the station name strike, dip, and slip. Solid lines are the observed seismograms, and dashed lines are the synthetic seismograms.

layered elastic medium overlying an elastic halfspace. After wavenumber integration, the convolution of Green's functions with the source–time function is done in the frequency domain. We calculated the Green's function for the crustal model used to locate the earthquake and using the source location obtained from the HYPOCENTER program. Rebollar *et al.* (1995) calculated a Q_β of 200 from acceleration records at BAHI. Assuming that $Q_\alpha/Q_\beta = 2$, a Q_α of 400 and a Q_β of 200 were used for the upper 4-km-thick layer. For deeper layers $Q_\alpha = Q_\beta = 2000$ was used. We calculated the ground displacement using a 3-sec triangular source–time function and a seismic moment of 1.28×10^{17} N m, estimated from the spectra of *Lg* waves (discussed below). We varied the strike from 300° to 360°, the dip from 60° to 90°, and the slip angle from $-180°$ to 180°. This range of variation of the source geometry was chosen to include the range of focal parameters encompassed by the first-motion and CMT solutions. In order to compare synthetic and observed seismograms, the observed seismograms were integrated and rotated, and both observed and synthetic seismograms were bandpass filtered between 0.1 and 0.05 Hz. The best match was obtained with the following fault geometry: $\phi = 330° \pm 15$, $\delta = 85° \pm 5$ and $\lambda = 165° \pm 15$. The fault-plane solution is shown in Figure 2c. The uncertainties are derived from the range of strike, dip, and slip that reasonably fit the observed seismograms. Figure 7 shows the comparison of synthetic and observed seismograms of BAHI, SAFE, and GUAY stations. The best match is obtained for the tangential component and a good agreement with the radial component of BAHI station. On the other hand, the vertical component

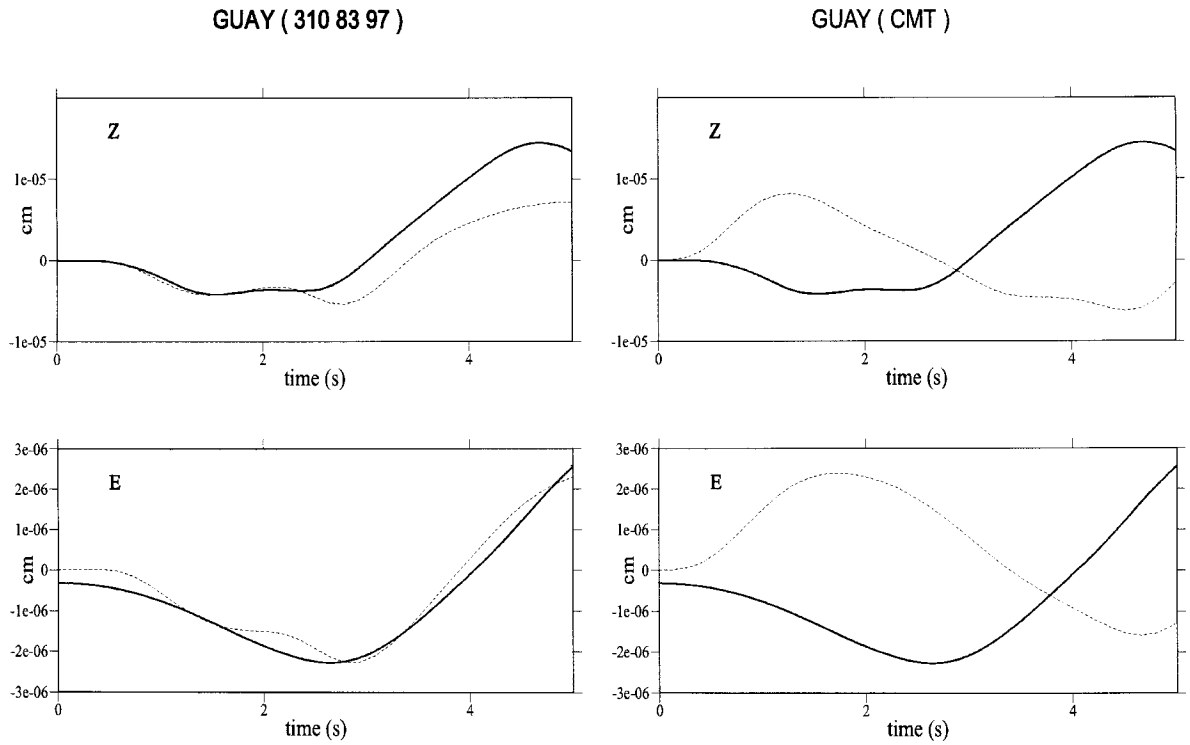

Figure 5. Comparison of observed and synthetic *P* waves calculated with the dip-slip geometry (left) and Harvard CMT (right) at GUAY station. At the top of the figure the station name, strike, dip, and slip are indicated. Solid lines are the observed seismograms and dashed lines are the synthetic seismograms. At this station only the vertical and east–west components were available.

does not show any agreement. The SAFE (160 km from the epicenter) and GUAY (371 km from the epicenter) stations show reasonable agreement, in this range of periods if we consider the source-station distances. We think that the mismatch between the observed and synthetics are because of vertical and lateral variations of the crustal structure in the Gulf of California. The Harvard centroid moment tensor (CMT) inversion reported a strike of 329°, a dip of 86°, and a slip of 172° with a centroid depth of 15 km. This solution is within the variation of our fits.

Lg-Wave Spectral Analysis

The NBT stations lie at distances from 140 to 270 km from the epicenter. Therefore, in this range of distances the *Lg* wave trains, rather than the *S* wave, are the most important features of the records. A prominent characteristic of the *Lg* wave phase is that it propagates along the continental crust. Gonzalez *et al.* (1998) and Lewis *et al.* (2001) found that the crustal structure in this region of the Gulf of California is a thinned continental crust. We estimated source parameters such as seismic moment (M_0), source radius (R), and stress drop ($\Delta\sigma$) from the spectra of the *Lg* phase following Xie (1998) and Reese *et al.* (1999). In this study, we assumed the ω^{-2} Brune (1970) source model. Thus the *Lg* displacement amplitude spectrum as a function of distance Δ and frequency f can be modeled by (Reese *et al.,* 1999):

$$A_i^{Lg}(f,\ \Delta) = \frac{M_0}{4\pi\rho\beta^3}\ \frac{1}{1 + \dfrac{f^2}{f_c^2}}\ \frac{1}{\sqrt{\Delta_0\Delta_i}}\ \exp\left(\frac{\pi f\Delta_i}{v_{Lg}Q_{Lg}(f)}\right), \quad (1)$$

where ρ is density, β is the shear-wave velocity, f is frequency, f_c is the corner frequency, $\sqrt{\Delta_0\Delta_l}$ is the geometrical spreading factor (Δ_0 is assumed to be 100 km) and Δ_l is the epicentral distance of the i-th seismic station, v_{Lg} is the mean *Lg* group velocity (assumed to be 3.4 km/sec), and $Q_{Lg}(f)$ is the Q of the *Lg* phase as a function of frequency.

The observed *Lg* displacement spectra were calculated from a time window that included the *Lg* wave train between group velocities from about 2.0 to 3.6 km/sec. The amplitude spectra were calculated from records of stations SAFE, ELAR, SACA, OBTO, ALAM, LOQI, and TELM (Fig. 8). Each individual spectrum was corrected for instrument response, geometrical spreading, and *Lg*-wave attenuation given by $Q_{Lg}(f) = 355f^{0.17}$, as obtained by Dominguez and Rebollar (1997) in the Peninsular Ranges. This attenuation relationship is valid from 1 to 6 Hz, but, we applied it to the whole range of frequencies. This correction raised the slope of the high-frequency spectral rolloff to -2, with only small

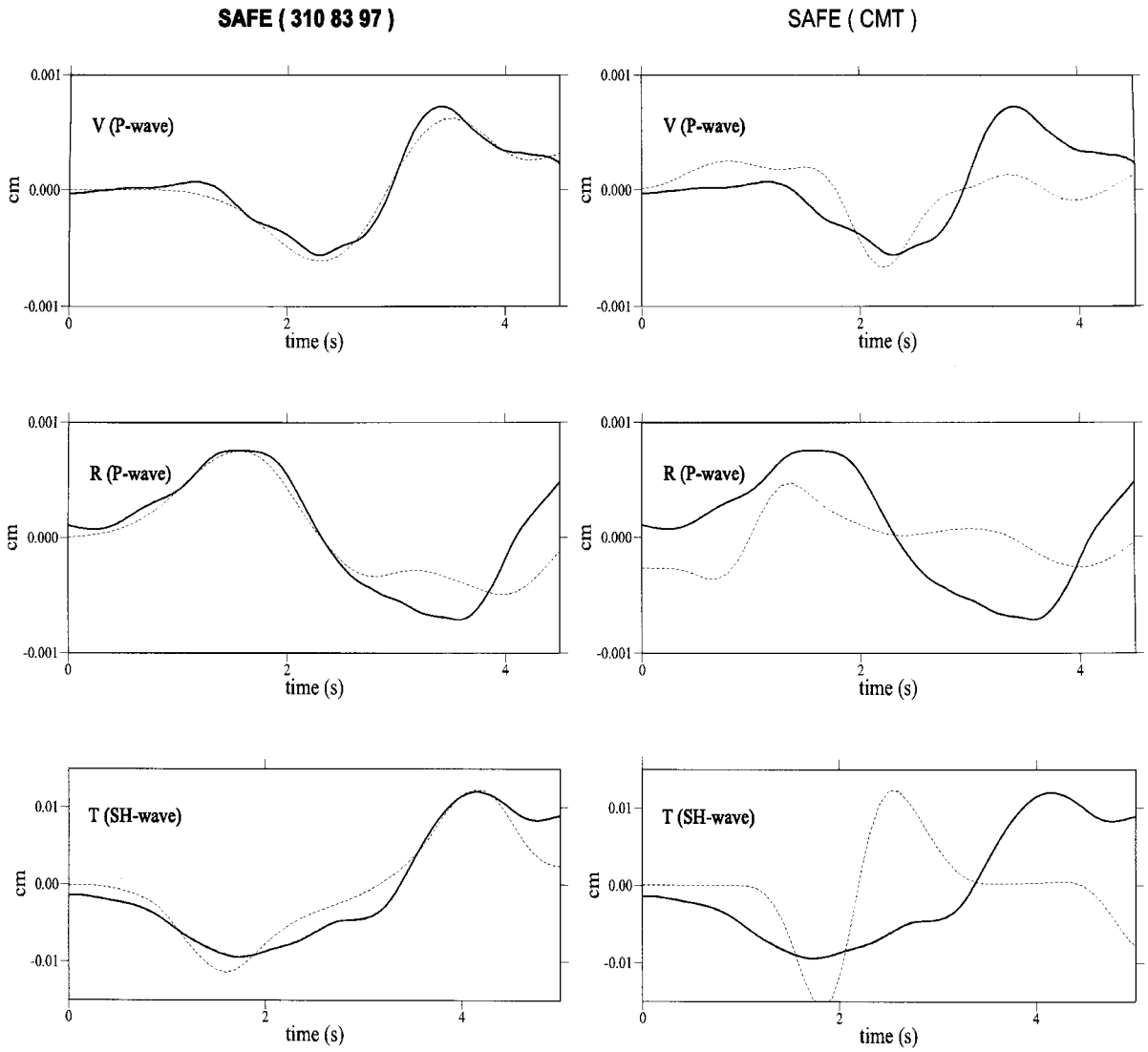

Figure 6. Comparison of observed and synthetic *P* waves calculated with the dip-slip geometry (left frame) and Harvard CMT (right frame) at station SAFE. At the top of the figure, the station name, strike, dip, and slip are indicated. Solid lines are the observed seismograms and dashed lines are the synthetic seismograms.

variations. Figure 9 shows the average displacement spectra and ± 1 standard deviation. A corner frequency of 0.2 Hz was inferred, and an average seismic moment of 1.28×10^{17} N m was calculated with equation (1). The source radius (R) and the stress drop ($\Delta\sigma$) were then calculated with the following relationships (Brune, 1970):

$$R = 0.3724 \frac{\beta}{f_c}, \tag{2}$$

$$\Delta\sigma = \left(\frac{7}{16}\right) \frac{M_0}{R^3}. \tag{3}$$

The resulting estimates give 6.3 km for the source radius and 0.22 Mpa (2.2 bars) for the stress drop. For comparison, we also used *S* waves recorded at the station BAHI to estimate the source parameters. A time window of 20 sec beginning at the arrival of the *S* wave was chosen to calculate the *S* wave spectra. This large time window included coda waves and surface waves. However, it was chosen that long in order to resolve the spectral amplitude at lower frequencies. The spectra were corrected for attenuation and instrumental response. In this case, the spectra were corrected using a Q_β of 200, independent of frequency, as estimated by Rebollar *et al.* (1995), from the analysis of the high-frequency spectral decay of the accelerograms recorded at BAHI. The spectra follow a ω^{-2} trend. A corner frequency of 0.21 Hz was estimated from the spectra shown in Figure 9. The estimated source parameters are a seismic moment of 3.00×10^{17} N m (3.00×10^{24} dyne cm); a source radius of 5.8 km, and a stress drop of 0.67 Mpa (6.7 bars). The

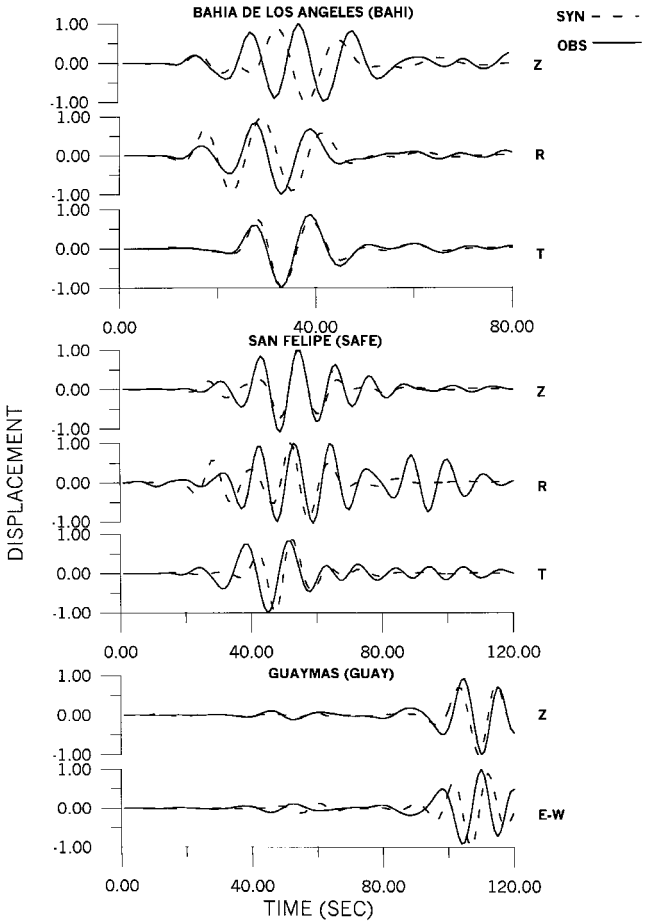

Figure 7. Comparison of observed surface waves and synthetics seismograms calculated with $\phi = 330°$, $\delta = 85°$, and $\lambda = 165°$ for stations BAHI, SAFE, and GUAY. Solid lines are the observed seismograms, and dashed lines are the synthetic seismograms. The best match is obtained for the tangential component of BAHI. All traces were normalized to one (see text for details).

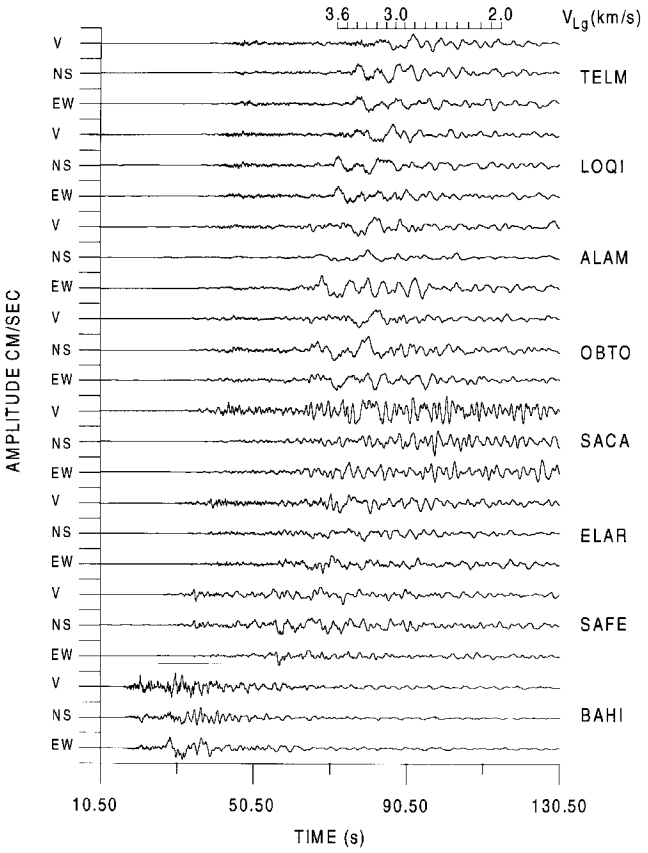

Figure 8. Plot of the seismograms recorded with the NBT seismic stations. The bar over the vertical component of the seismogram at TELM indicates group velocity and time window used in the spectral analysis of the *Lg* wave. The bar over the vertical component of the seismogram for station BAHI indicates the time window used to calculate the spectra of the *S* waves.

source radius and stress-drop estimates compare well with those obtained with *Lg* displacement spectra. The discrepancy in moment is probably attributable, at least in part, to the fact that the time window includes some contributions from surface waves in addition to the *S* wave.

Discussion and Conclusions

In the effort to study the seismic activity of the Gulf of California since the late 1960s (Lomnitz *et al.,* 1970; Brune *et al.,* 1976), this is the first time that a moderate size earthquake was well recorded in the Gulf of California extensional province. The 5.5 magnitude event that occurred on 26 November 1997 generated a high-quality seismic data set. The event was recorded by permanent and portable broadband seismic stations as well as by the short period RESNOM seismic network. This event was located in the intersection of the Delfin spreading center and the transform fault that joins the upper and lower Delfin basins at a depth of 5 km (see Fig. 1). Body- and surface-wave modeling also constrained the depth at 5 km. The fault plane solution calculated using first arrivals indicate dip-slip ($\phi = 310°$, $\delta = 83°$, $\lambda = 97$). On the other hand, the synthetic waveform modeling of surface waves performed with local seismic stations and the Harvard CMT inversion ($\phi = 329°$, $\delta = 86°$, $\lambda = 172°$) indicates a right lateral strike-slip fault. The initial reverse faulting was corroborated by body-wave modeling of the first arrivals of the BAHI, SAFE, and GUAY stations. Waveform modeling of surface waves recorded with local seismic stations resulted in a fault geometry given by a strike of $330° \pm 15$, dip of $85° \pm 5$ and slip of 165 ± 15. This is a right lateral strike-slip fault and agrees, within the uncertainties, with the Harvard CMT inversion. The hypocentral location and the result of the wave modeling indicates that this is a complex event originated in the pull-apart Delfin basin. It is possible that the initial faulting started as a dip-

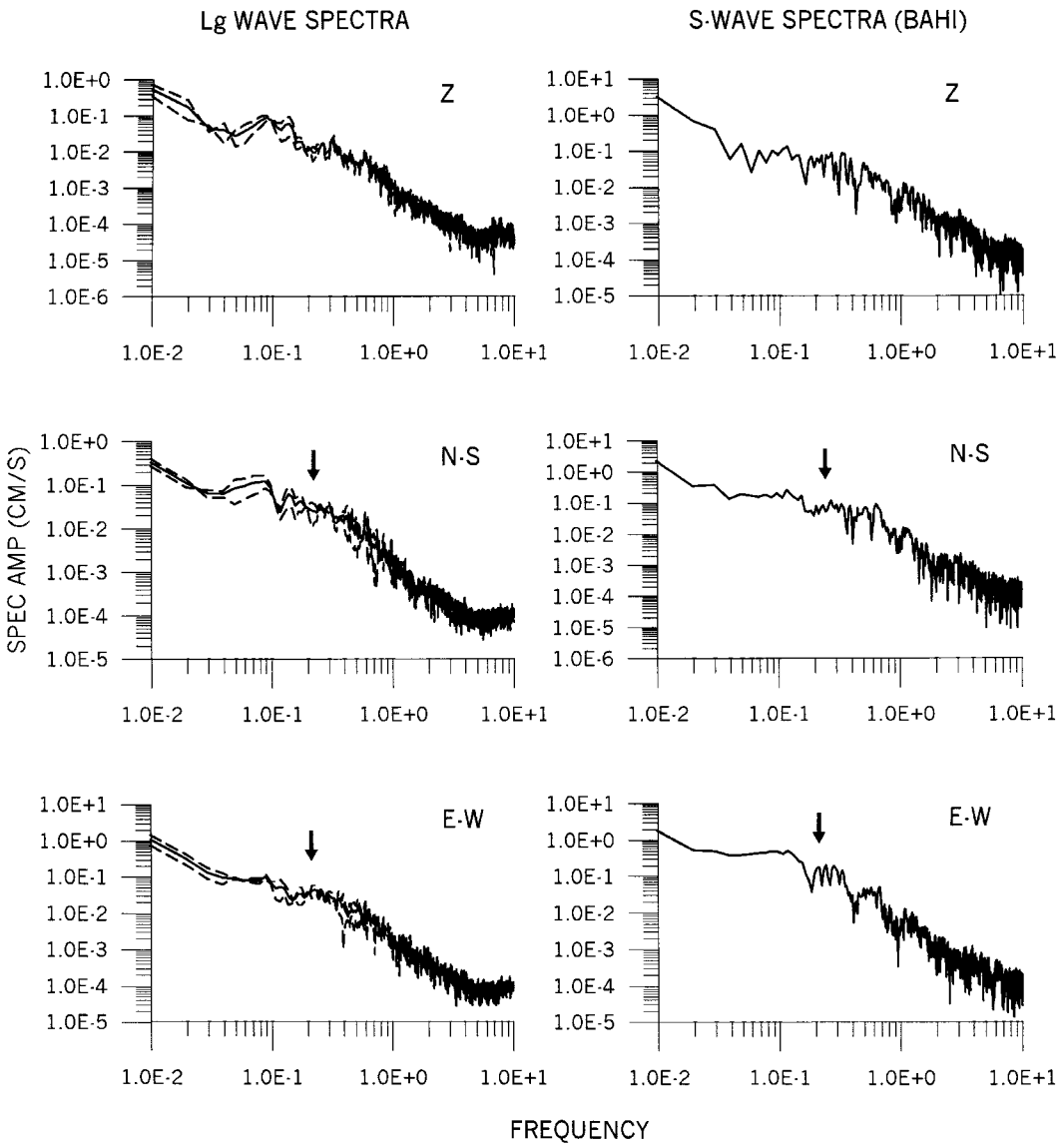

Figure 9. Right frames are the average *Lg*-displacement spectra (continuous line) and ± 1 standard deviation (dashed line). Left frames are the *S*-wave displacement spectra from the event recorded at BAHI station. We corrected the spectra using a frequency independent Q_β of 200 (Rebollar *et al.,* 1995).

slip reverse fault and ended releasing the bulk of energy as a strike-slip fault.

The *P* and *T* axes in both mechanisms, dip-slip and right lateral strike slip, are roughly in the northwest and southeast direction. Therefore, the *P* and *T* axes indicate the local stress orientation at this edge of the spreading center. The *P* and *T* axes from the 6.5 magnitude Canal de Balienas seismic event of 8 July 1975 (Munguia *et al.,* 1977) lie in the north–south direction and are interpreted to reflect the regional stress environment.

From the spectra of *Lg* waves recorded at seven stations on the Peninsular Ranges, we calculated source parameters. In the analysis we assumed the ω^{-2} Brune (1970) source model and an attenuation $Q_{Lg}(f)$ as a function of frequency calculated for the Peninsular Ranges (Dominguez and Rebollar, 1997). A seismic moment of 1.28×10^{17} N m was calculated from the displacement spectra of *Lg* waves. The observed corner frequency of 0.2 Hz is equivalent to a source radius of 6.3 km and gives a Brune's stress drop of 2.2 bars. This low stress drop is evident in the seismograms, since low frequencies dominate the seismic records. This stress drop contrasts with the high stress drop of the Bahla de Las Animas event of magnitude 5.5 that occurred on 5 April 1993 30 km south of Bahla de Los Angeles (Rebollar and Castillo, 1994; Rebollar *et al.,* 1995). This normal fault event generated a maximum acceleration of 101 gal and had a calculated stress drop of 95 bars. The difference between the tectonic environments where these earthquakes occurred

suggests that the crust at the Delfin Basin may not be capable of sustaining high stresses as is usually suggested (Scholz, 1990).

Acknowledgments

We would like to thank Antonio Mendoza, Arturo Perez-Vertti, Oscar Galvez, Luis Orozco, and Luis Inzunza who helped us in the field maintenance of the seismic stations. Antonio Mendoza and Jennifer Eakins helped us greatly in the management of the digital data. Jose Pujol and an anonymous reviewer provided helpful suggestions. We thank the Southern California Earthquake Center and the IRIS-PASSCAL program for loaning us some of the instrumentation used in this study. This project was sponsored by the CICESE internal projects and CONACYT (F360-T93302 and 28458-T).

References

Brune, J. N. (1970). Tectonic stress and the spectra of seismic shear waves from earthquakes. *J. Geophys. Res.* **75,** 4997–5009.

Bouchon, M. (1981). A simple method for calculating Green's functions for elastic layered media, *Bull. Seism. Soc. Am.* **71,** 959–972.

Dominguez, T., and C. J. Rebollar (1997). Regional variations of seismic attenuation from coda and Lg waves in northern Baja California. *J. Geophys. Res.* **102,** 15,259–15,268.

Goff, J. A., E. A. Bergman, and S. C. Solomon (1987). Earthquake source mechanism and transform fault tectonics in the Gulf of California. *J. Geophys. Res.* **92,** 10,485–10,510.

González, A., J. J. Dañobeitia, D. Córdoba, L. A. Delgado-Argote, R. Bartolomé, and F. Michaud. (1998). Estructura sísmica y gravimétrica de la corteza en el norte del Golfo de California (abstract). *GEOS Unión Geofísica Mexicana* **18,** 292.

Herrmann, R. B. (1987) *Computer Programs in Seismology,* St. Louis University, St Louis, Missouri.

Herrmann, R. B., and C. Y. Wang (1985). A comparison of synthetic seismograms, *Bull. Seism. Soc. Am.* **75,** 41–56.

Lee, W. H. K., and J. C. Lahr (1972). HYPO71: a computer program for determining hypocenter, magnitude, and first motion pattern of local earthquakes, *U. S. Geol. Surv. Open-File Rept.*

Lewis, J. L., S. M. Day, H. Magistrale, R. Castro, L. Astiz, C. J. Rebollar, J. Eakins, F. Vernon, and J. N. Brune (2001). Crustal thickness of the Peninsular Ranges and Gulf Extensional Province in the Californias. *J. Geophys. Res.* (submitted).

Lienert, B. R., E. Berg, and L. N. Frazer (1988). HYPOCENTER: an earthquake location method using centered, scaled, and adaptively least squares. *Bull. Seism. Soc. Am.* **76,** 771–783.

Lienert, B. R., and J. Havskov (1995). A computer program for locating earthquakes both locally and globally. *Seism. Res. Lett.* **66,** 26–36.

Lomnitz, C., F. Mooser, C. R. Allen, J. N. Brune, and W. Thatcher (1970). Seismicity and tectonics of the northern Gulf of California, Mexico: preliminary results, *Geofisica Internacional* **10,** 37–48.

Lonsdale, P. L. (1989). Geology and tectonics history of the Gulf of California, in *The Geology of North America: The Eastern Pacific Ocean and Hawaii,* vol. N, The Geological Society of America.

Mungula, L., M. Reichle, A. Reyes, R. Simons, and J. N. Brune (1977). Aftershocks of the 8 July, 1975 Canal de Ballenas, Gulf of California, earthquake, *Geophys. Res. Lett.* **4,** 507–509.

Reasenberg, P., and D. Oppenheimer (1985). FPFIT, FPPLOT, and FPPAGE: Fortran computer programs for calculating and displaying earthquake fault-plane solutions, *U.S. Geol. Surv. Open-File Rept. 85-739.*

Rebollar, C. J., and J. Castillo (1994). Seismicity at the Delfin Ridge, Canal de Ballenas transform fault and Salsipuedes Ridge of the Gulf of California, Mexico (abstract), in *EOS Spring Meeting,* 241.

Rebollar, C. J., J. Castillo-Roman, and A. Uribe (1995). Parametros de fuente de la actividad sismica que ocurrio en marzo de 1993 en la Bahia de las Animas, Baja California. Monografia No 2 Union Geofisica Mexicana, Vol. 2, 229–235.

Reichle, M. S., and I. Reid, (1977). Detailed study of earthquake swarms from the Gulf of California, *Bull. Seism. Soc. Am.* **67,** 159–171.

Reese, C. C., R. R. Rapine, and J. F. Ni (1999). Lateral variations of Pn and Lg attenuation at the CDSN station LSA, *Bull. Seism. Soc. Am.* **89,** 325–330.

Reyes, L. M., C. J. Rebollar, and R. Castro (2001). Depth of the Moho in Northern Baja California using (P_g-P_n) travel times. *Geofisica Internacional* (in press).

Scholz, C. H. (1990). The mechanics of earthquakes and faulting, Cambridge University Press, New York, 298.

Stock, J. M., and K. V. Hodges (1989). Pre-Pliocene extension around the Gulf of California and transfer of Baja California to the Pacific plate. *Tectonics* **8,** 99–115.

Tajima, F., and D. M. Tralli (1992). Variations of seismic slip in the Gulf of California and possible effects on geodetic measurements of the Pacific-North American plate motion, *J. Geophys. Res.* **97,** 4903–4913.

Thatcher, W., and J. N. Brune (1971). Seismic study of an oceanic ridge earthquake swarm in the Gulf of California, *Geophys. J. R. Astr. Soc.* **22,** 473–489.

Thatcher, W., and J. N. Brune (1973). Surface waves and crustal structure in the Gulf of California region. *Bull. Seism. Soc. Am.* **63,** 1689–1698.

Wang, C. Y., and R. B. Herrmann (1980). A numerical study of P-SV and SH-wave generation in plane layered medium, *Bull. Seism. Soc. Am.* **70,** pp. 1015–1036.

Xie, J. (1998). Spectral inversion of Lg from earthquakes: a modified method with applications to the 1995, Western Texas earthquake sequence, *Bull. Seism. Soc. Am.* **88,** 1525–1537.

Department Sismología
División Ciencias de la Tierra
Centro de Investigación Cientifica y de Educación Superior
de Ensenada (CICESE)
(C.J.R., R.R.C., J.M.)

Instituto de Geofisica
UNAM
(L.Q.)

Scripps Institution of Oceanography
University of California–San Diego (UCSD)
La Jolla, California
(L.A., F.V.)

Department of Geological Sciences
San Diego State University (SDSU)
San Diego, California
(S.M.D.)

Seismological Laboratory
University of Nevada
Reno, Nevada
(J.N.B.)

Manuscript received 31 May 2000.